Composite Structures 248 (2020) 112496

Contents lists available at ScienceDirect

Composite Structures

journal homepage: www.elsevier.com/locate/compstruct

Energy dissipation in adhesive and bolted pultruded GFRP double-lap joints under cyclic loading

Ghazaleh Eslami, Sonia Yanes-Armas, Thomas Keller *

Composite Construction Laboratory (CCLab), École Polytechnique Fédérale de Lausanne (EPFL), Switzerland

ARTICLE INFO

Keywords:
Energy dissipation
Cyclic loading
Adhesive joints
Bolted joints
Flexible adhesive

ABSTRACT

Fiber-reinforced polymer (FRP) structures, due to their low mass, are valuable alternatives to traditional steel or concrete structures in seismic areas. However, to resist seismic actions, FRP structures must be able to dissipate a significant amount of inelastic energy. Since FRP materials are brittle, this dissipation must occur in the joints. Monotonic tension and cyclic tension–compression experiments were thus performed on adhesive and bolted double-lap joints composed of pultruded glass fiber-reinforced polymer (GFRP) profiles; a flexible adhesive was used in the adhesive joints. A significant amount of energy was dissipated in the adhesive joints at lower and medium displacement rates through viscoelastic friction and damage in the adhesive, while almost no energy dissipation occurred at the highest rate. The energy in the bolted joints was dissipated by progressive crushing and shear-out failures in the inner laminates. Although the dimensions and monotonic strength of the adhesive and the bolted joints were similar, the former dissipated significantly more energy at the two lower applied displacement rates. The obtained results can contribute to the seismic design of inelastic joints in FRP structures.

1. Introduction

Fiber-reinforced polymer (FRP) composites are characterized by their high specific strength and stiffness and are thus ideally suited for lightweight construction. Their lightweight, i.e. their low mass, also provides an advantage in resisting earthquake actions since the inertial forces are reduced. However, an efficient earthquake-resistant structural design also requires a high inelastic energy dissipation capacity and in this respect, FRP composites are less appropriate due to their brittle behavior.

Possibilities for overcoming brittle material behavior do exist however, e.g. by implementing an inelastic energy dissipation capacity on the structural system level, i.e. by implementing system ductility or system pseudo-ductility (instead of material ductility) [1]. Ductility and pseudo-ductility are mainly differentiated by the formation of irreversible damage, which only occurs in the latter case. System ductility can be achieved by combining brittle and ductile members in a structure, e.g. a glass-FRP (GFRP) bridge deck with steel girders [2], where inelastic energy is dissipated by the ductile members. In a structure composed of only brittle members, pseudo-ductility can be obtained by designing redundant (statically indeterminate) structural systems, which enable progressive failure of the brittle members and thus dissipation of inelastic energy [3].

Specific ''members'' that can dissipate inelastic energy through ductile or pseudo-ductile failure mechanisms are the joints between structural members. System ductility or pseudo-ductility can be achieved for instance by using flexible adhesives [1,4]. The adhesive layer may dissipate inelastic energy through viscoelastic friction, plasticity or damage. Since such adhesives are flexible however, their behavior is strain rate-dependent and their energy dissipation capacity strongly depends on the applied strain or loading rate [4,5]. Furthermore, bolted joints can exhibit a pseudo-ductile behavior in the case of FRP members, if bearing (crushing) failure occurs, which is activated by appropriately selecting the edge distances of the bolts and thus preventing brittle shear-out or net-tension failure mechanisms [6,7].

Similar to FRP structures, timber and cold-formed steel (CFS) structures may behave in a brittle manner, for different reasons however. The reason in the first case is, as for FRP materials, the brittle behavior of timber. In the second case, although the material is ductile, pre-yield local buckling of the thin CFS sheets can occur and lead to a

* Corresponding author.
E-mail addresses: ghazaleh.eslami@epfl.ch (G. Eslami), sonia.yanesarmas@epfl.ch (S. Yanes-Armas), thomas.keller@epfl.ch (T. Keller).

https://doi.org/10.1016/j.compstruct.2020.112496
Received 10 March 2020; Revised 14 May 2020; Accepted 15 May 2020
Available online 19 May 2020
0263-8223/

brittle failure nevertheless. To achieve system ductility in timber buildings, glued-in steel rod connections can provide a high energy dissipation capacity at each cycle after the yielding of the rods [8,9]. In the case of CFS sections, the activation of bolt slippage prior to local buckling, in bolted connections, can significantly improve the energy dissipation capacity [10,11].

Only a limited amount of research has been performed on the cyclic energy dissipation capacity of structures composed of FRP members. Due to the elastic-brittle behavior of FRP members, the potential energy dissipation in an FRP frame structure is mainly concentrated in its connections [12]. Studies of the cyclic performance of bonded steel sleeve connections for joining tubular GFRP beams and columns were conducted in [13,14], in terms of their ductility and energy dissipation capacity. The joint experiments showed that excellent ductility and energy dissipation capacity could be achieved through the yielding of the steel endplates before the final connection failure. Another experimental and numerical investigation of the cyclic behavior of a novel tubular GFRP beam-to-column sleeve connection system was conducted in [15]. Several bolt configurations were studied and it was found that increasing the edge distance of the bolts leads to a significant enhancement of the hysteretic behavior of the connections. It should be noted that no previous studies were found on the energy dissipation in adhesive joints composed of FRP members and flexible adhesives, subjected to cyclic loading, and their performance comparison to bolted joints.

In this work, a series of monotonic tension and reversed cyclic loading experiments was designed and conducted to study and compare the load–displacement behavior and the energy dissipation capacity of adhesive and bolted GFRP double-lap joints. The applied cyclic loading was considered as being able to simulate a deformation history to which light-frame buildings are likely to be subjected during earthquakes. A flexible adhesive and stainless-steel bolts were used to connect the brittle GFRP profiles. The joints were designed to have similar geometry and monotonic strength to allow the comparison of energy dissipation during cyclic loading. Further parameters of the investigation were the applied displacement rate in the case of the adhesive joints and the bolt configuration in the case of the bolted joints.

2. Experimental set-up

2.1. Joint geometry and preparation

Double-lap joints were selected to minimize the eccentricities; the joints consisted of two outer laminates of 230 mm length and 100 mm width and an inner laminate of 200 mm length and 100 mm width; all three laminates were of 10 mm thickness, see Fig. 1. The outer laminates thus bore only half of the load of the inner laminate. A laminate piece of 85 × 100 × 10 mm was placed between the outer laminates at the joint end where the axial displacement was applied by the machine grips; the other joint end, i.e. the inner laminate, was directly fixed in the machine. The compact joint configuration was chosen in order to prevent buckling during the compression cycles. Due to the high deformability of the adhesive, the stress distribution was nevertheless uniform along and across the joint overlaps; the local load transfer mechanism in the bolted joints was not affected by the vicinity of the machine grips either.

The overlap length of the adhesive joints was 100 mm. The adhesive thickness was selected as 5 mm, to be representative of typical applications in GFRP bridge and building construction [2,16]. Two types of bolted joints were studied: four-bolt and two-bolt joints. The overlap length of the two-bolt joints was 100 mm and thus identical to that of the adhesive joints, while that of the four-bolt joints was 110 mm. The diameter of the bolts was 10 mm, i.e. identical to the laminate thickness, and thus fulfilling the condition in [6]; the bolt hole clearance was 1 mm. To prevent early shear-out failure, the distances between the centerlines of bolts and laminate edge (a in Fig. 1), and between the two rows of bolts (a'), were selected as being 3.5× and 4× the bolt diameter, respectively, in the four-bolt joints, according to [6]. In the two-bolt joints, the laminate length between bolts and laminate edge of the inner laminate was thus doubled from 30 to 60 mm. In the transverse direction, the edge distance was 2.5× the bolt diameter in all bolted joints.

2.2. Materials

The GFRP laminates were pultruded by Fiberline, Denmark. They were composed of E-glass fibers and an isophthalic polyester resin matrix with a fractional fiber weight of 60%. The laminate architecture consisted of approximately 70% unidirectional rovings in the central part and two outer combined mats. A polyester surface veil covered the outsides. The corresponding measured longitudinal elastic modulus was 33.3 ± 0.7 GPa and the tensile strength 240 MPa (manufacturer data).

The adhesive was a flexible structural two-part system based on acrylic double performance (ADP) polymer technology, SikaFast®-5221 NT, supplied by Sika, Switzerland. The two components (SikaFast5221NT and SikaFast5200) were mixed at a ratio of 10:1 (by volume). The adhesive, whose response is highly rate-dependent, exhibits pseudo-ductile behavior at low and moderate displacement rates [17]. Elastic moduli of 140 MPa up to 368 MPa were measured on standardized dogbone specimens at 0.03 mm/s up to 0.83 mm/s displacement rates [17].

Grade 80 stainless steel bolts M10 were used, with an unthreaded length of 35 mm. The nuts were hand-tightened to prevent the bolts from being pre-stressed.

2.3. Adhesive joint manufacturing

The surface of the GFRP laminates was firstly roughened with sandpaper to remove the polyester surface veil until the combined mat layer was revealed at an approximately 0.5 mm depth. Based on preliminary experiments, to avoid early adhesion failure, a thin epoxy adhesive layer (of approximately 0.5 mm thickness, Sikadur-330) was applied as an adhesion promoter and cured for four hours at 60 °C [17]. The two-part ductile adhesive was then applied using a mixing gun, and four steel beads of 5 mm diameter were placed in the bonding area to guarantee the targeted layer thickness. One-day curing under ambient laboratory conditions (21 ± 3 °C and 38 ± 10% relative humidity) was applied for each lap. Subsequently, the joint was stored for five days in the same room prior to the experiments.

2.4. Instrumentation

The joint axial and through-thickness deformations were measured, in monotonic and cyclic experiments, by a video-extensometer, at a rate of 10 Hz and ± 0.003 mm to ± 0.015 mm accuracy. The distances and the numbering of the corresponding measuring points on the laminate side faces are shown in Fig. 2, (a) for adhesive, (b) four-bolt, and (c) two-bolt joints. Additional points were fixed on the bolt heads (nos. 22 and 23 in four-bolt and 19 in two-bolt joints) and at the ends of the inner laminates (no. 24 in four-bolt and 20 in two-bolt joints). These additional points allowed to derive the laminates' crushing deformations from the differential displacements of the target pairs 8–22 and 14–23 in four-bolt, and 8–19 in two-bolt joints. Similarly, the shear-out deformations could be obtained from the target pairs 20–24 and 17–20 in the four- and two-bolt joints respectively, see Fig. 3. The loads and total specimen displacements

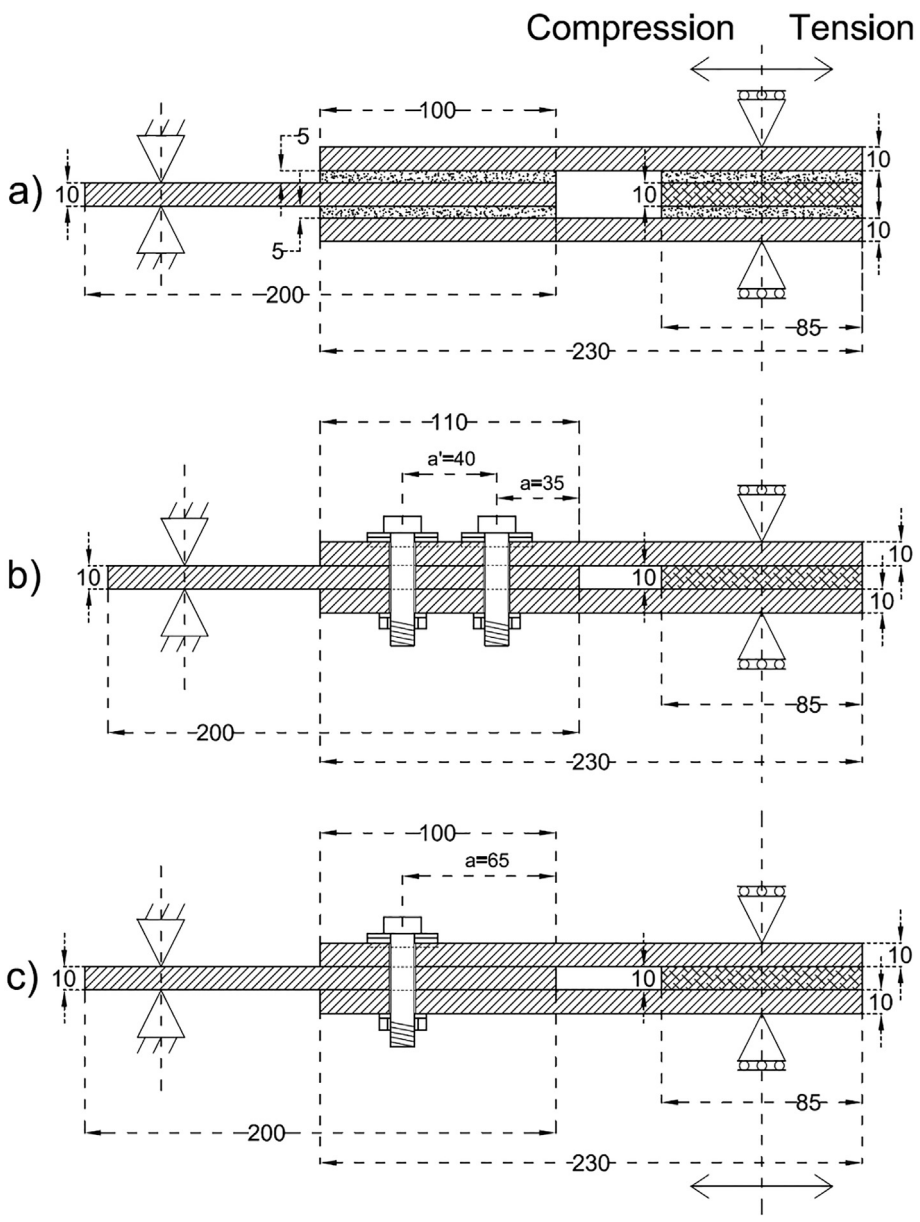

Fig. 1. Specimen dimensions (mm) in longitudinal section of a) adhesive, b) four-bolt, c) two-bolt joint (two bolts across the width in each case).

were also measured by the loading machine at a rate of 100 Hz for the specimens at 1 mm/s displacement rate (see below), and 10 Hz for the remaining specimens.

2.5. Experimental program

Monotonic tension and cyclic tension–compression experiments were performed on all joint types. Since cyclic loading protocols for GFRP joints do not yet exist, a protocol developed for joints in timber frames was selected, i.e. the CUREE protocol [18], which is also included in the ASTM E2126 standard [19], specified there as "Test Method C". The protocol is a "realistic and conservative representation of the cyclic deformation history to which a component of a wood structure likely is subjected in earthquakes" (citation from [19]).

According to [18] and [19], the reference displacement or amplitude of the applied cycles, Δ, is defined based on the load–displacement curves obtained from monotonic experiments. The reference displacement is equal to 60% of the joint displacement at 80% of the maximum load, F_{max}, taken in the after-peak softening branch, $\Delta_{0.8Fmax}$. The applied load history then consists of primary cycles, whose amplitude is a fraction of Δ, and intermediate trailing cycles (two after the initial phase) of 75% of the amplitude of the previous primary cycle, see Fig. 4.

As far as the displacement rate is concerned, in [18] reference is made to ISO 16,670 [20], where values between 0.1 and 10 mm/s are recommended. In view of the high rate sensitivity of the adhesive and the results obtained in [17], three displacement rates of 0.1, 0.5 and 1.0 mm/s were selected for the adhesive joints, in monotonic and cyclic experiments, denominated low, medium and high rate in the following. Consequently, the effect of the displacement rate on the energy dissipation capacity of the adhesive joints was also evaluated. The bolted joints were subjected to only one rate, i.e. the lowest, 0.1 mm/s, since the sensitivity to the displacement rate was considered to be much less than that of the adhesive joints, in view of the approximately 100× higher elastic modulus of the GFRP laminates compared to that of the adhesive and their mainly unidirectional

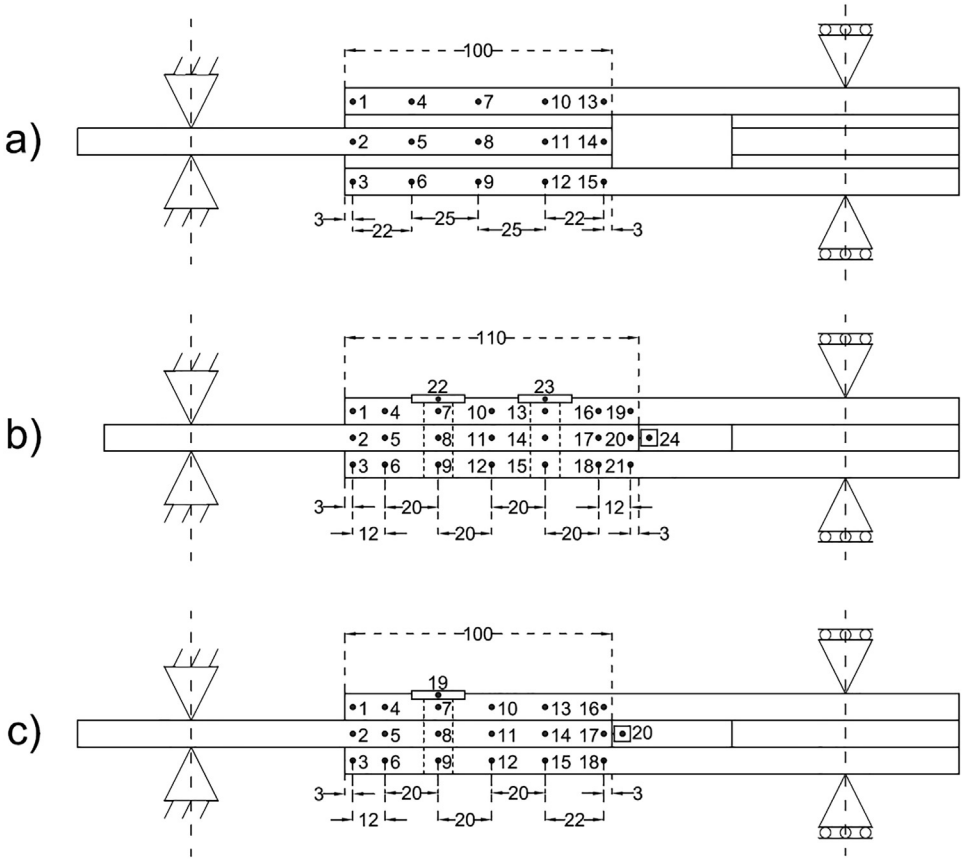

Fig. 2. Video-extensometer target points and distances (mm), a) adhesive, b) four-bolt, c) two-bolt joints.

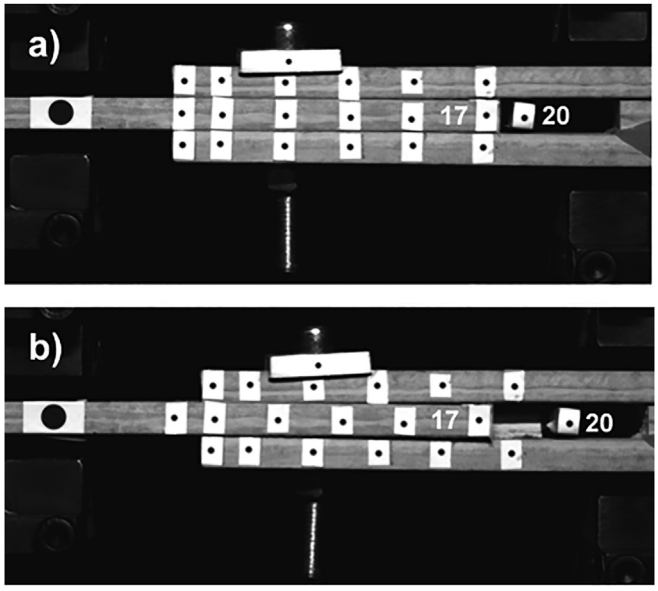

Fig. 3. Shear-out deformation measured by targets 17 and 20 in two-bolt joints, a) initial target positions, b) target positions after shear-out failure.

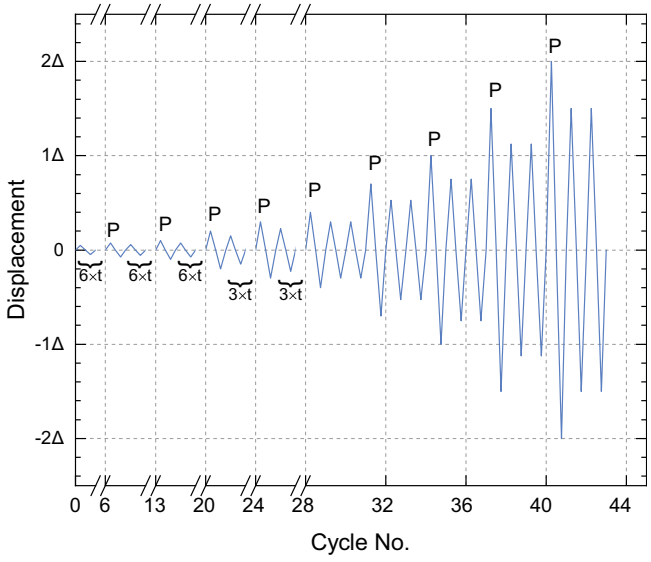

Fig. 4. Cyclic displacement scheme [19] (P = primary cycle, t = trailing cycle).

architecture. Selecting the lowest rate also provided the most favorable condition in view of high energy dissipation.

The displacement rate was applied by the machine to the whole specimen and thus included the small elastic deformation of the laminates outside of the joint; the rate applied to the joint part was thus insignificantly lower. Since the displacement rate was kept constant during each experiment, the frequency of the cycles varied and decreased during the experiments due to the increase of the displacement amplitudes, see Fig. 5.

Two experiments were performed for each parameter combination in monotonic and cyclic investigations. The joint denominations included the joint type (A, B4 or B2), loading type (S or C), rate

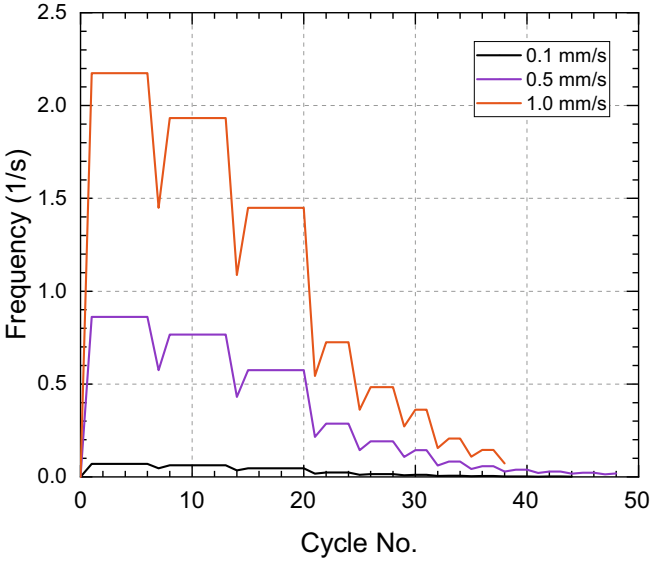

Fig. 5. Frequency variations during cyclic scheme for each type of specimen.

(0.1, 0.5, 1.0) and joint replicate (a or b). '' B4-C0.1a" for instance indicates the first four-bolt joint under cyclic loading at a rate of 0.1 mm/s, while ''A-S1.0b" denominates the second adhesive joint under monotonic (static) loading at a rate of 1.0 mm/s.

A Walter + Bai type LFV universal experimental machine was used with a capacity of 200 kN in tension and compression and a maximum displacement of 200 mm. Both monotonic and cyclic experiments were conducted in a laboratory environment at ambient temperature (21 ± 3 °C).

3. Experimental results

3.1. Monotonic experiments

3.1.1. Adhesive joints

The load-joint displacement responses of the adhesive joints under monotonic loading are shown and summarized in Fig. 6 and Table 1. The joint displacements were obtained from the target pairs 2–13, see Fig. 2; the joints exhibited a bilinear behavior. The displacement rate significantly influenced the initial (tangential) stiffness, S, the yield load, F_y (determined as the intersection of two tangent lines to the almost linear segments), and the displacement at failure, Δ_{fail}, the former two increasing and the latter decreasing as the rate increased from 0.1 to 1.0 mm/s. The remaining results, i.e. yield displacement, Δ_y, and maximum load, F_{max}, exhibited only a slight dependency on the rate. The highest maximum loads and maximum displacements at failure were achieved at the low rate. At the low rate, furthermore, a significant hardening occurred in the second part of the curves between yield and maximum load. The two joints per configuration exhibited similar and consistent behaviors.

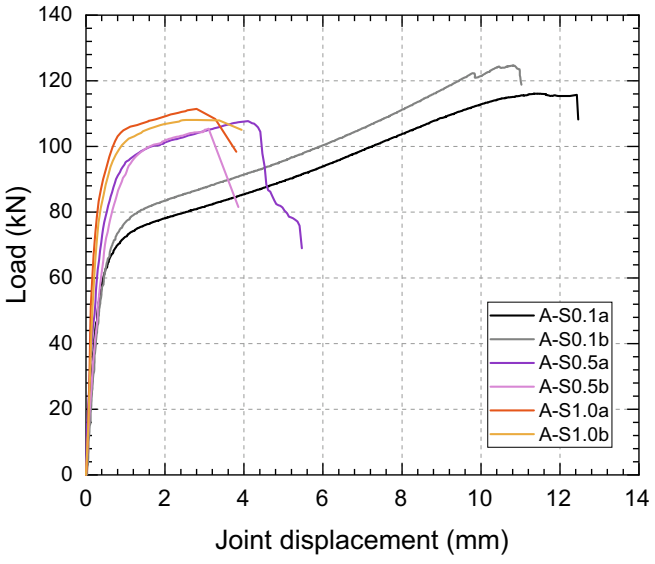

Fig. 6. Load-joint displacement responses of adhesive joints.

The shear strain distributions in the adhesive layers were derived from the through-thickness target pairs; they are shown in Fig. 7 at three load levels, i.e. below and at the yield load and at the maximum load. The resulting strain distributions were almost uniform at all load levels and did not exhibit peaks at the overlap ends (typical for stiffer, e.g. epoxy adhesives). The through-thickness strains were also derived, but they were small, only approximately 10% of the shear strains, and are thus not shown.

Failure of all joints occurred in the inner laminate. The failure mode was a fiber-tear failure according to [21]; Fig. 8 shows the failure plane, located within the visible combined mats of the inner laminate. The failure mode was not affected by the displacement rate.

3.1.2. Bolted joints

The load-joint displacement responses and results obtained for the bolted joints under monotonic loading are shown in Fig. 9 and summarized in Table 1. The joint displacements were obtained from the target pairs 2–19 and 2–16 for the four- and two-bolt joints, see Fig. 2. Also shown in Fig. 9 are the points of crushing and shear-out initiation (indicated by star and square symbols). In both four- and two-bolt joints, the load-joint displacement curves consisted of five segments, (i) clearance compensation up to approx. 1 mm of displacement, (ii) linear behavior up to crushing initiation, (iii) stiffness reduction during crushing up to shear-out initiation, (iv) further stiffness reduction during simultaneous crushing and shear-out up to the maximum load, and (v) significant drop of the load during only small displacements in the four-bolt and more significant displacements in the two-bolt joints.

Crushing initiation occurred simultaneously in both rows of the four-bolt joints. They exhibited a much stiffer behavior after crushing initiation and higher maximum loads (38% on average) than two-bolt joints since the bolts in the former transferred only half of the load of the latter and crushing and shear-out initiation thus occurred at higher loads. The crushing deformations up to failure in the four-bolt case were less than half of those of the two-bolt case, as shown in Fig. 10; the shear-out deformations before failure were however similar. After the maximum load, crushing no longer occurred. The combined crushing/shear-out failure modes of both joint types are shown in Fig. 11. Failure occurred only in the inner laminates, the outer laminates remained undamaged since they bore only half of the load. The steel bolts also remained undamaged.

3.1.3. Derivation of cyclic reference displacements

The cyclic reference displacements, Δ, were derived from the monotonic experiments, as described above. Since no clear softening behavior was obtained and values $\Delta_{0.8Fmax}$ in the softening branches could thus not be determined, the 60% fraction was applied to Δ_{fail}, see Table 1. In the latter values, the clearance of the bolted joints was discounted. The average Δ values of both specimens were taken as reference and applied in the cyclic experiments, see Table 2.

3.2. Cyclic experiments

3.2.1. Adhesive joints

The load-joint displacement responses of the adhesive joints under cyclic loading are shown in Fig. 12. One of the two specimens of each displacement rate was selected (which both showed consistent

Table 1
Results obtained from monotonic experiments for adhesive and bolted joints.

Joint	S (kN/mm)	Δy (mm)	F_y (kN)	F_{max} (kN)	Δ_{fail} (mm)	Δ (mm)
A-S0.1a	200.3	0.40	71.8	116.1	12.6	7.6
A-S0.1b	192.2	0.42	77.4	124.6	11.1	6.7
A-S0.5a	231.7	0.36	95.3	107.7	5.6	3.4
A-S0.5b	210.8	0.37	95.6	105.3	3.9	2.4
A-S1.0a	364.6	0.32	102.9	111.8	3.8	2.3
A-S1.0b	307.9	0.33	103.2	108.1	3.9	2.3
B4-S0.1a	52.2	–	–	123.9	2.7	1.6
B4-S0.1b	54.4	–	–	115.4	2.8	1.7
B2-S0.1a	43.5	–	–	88.0	5.1	3.1
B2-S0.1b	43.7	–	–	84.8	4.8	2.9

Note: 1-mm clearance was discounted in Δ_{fail} of bolted joints.

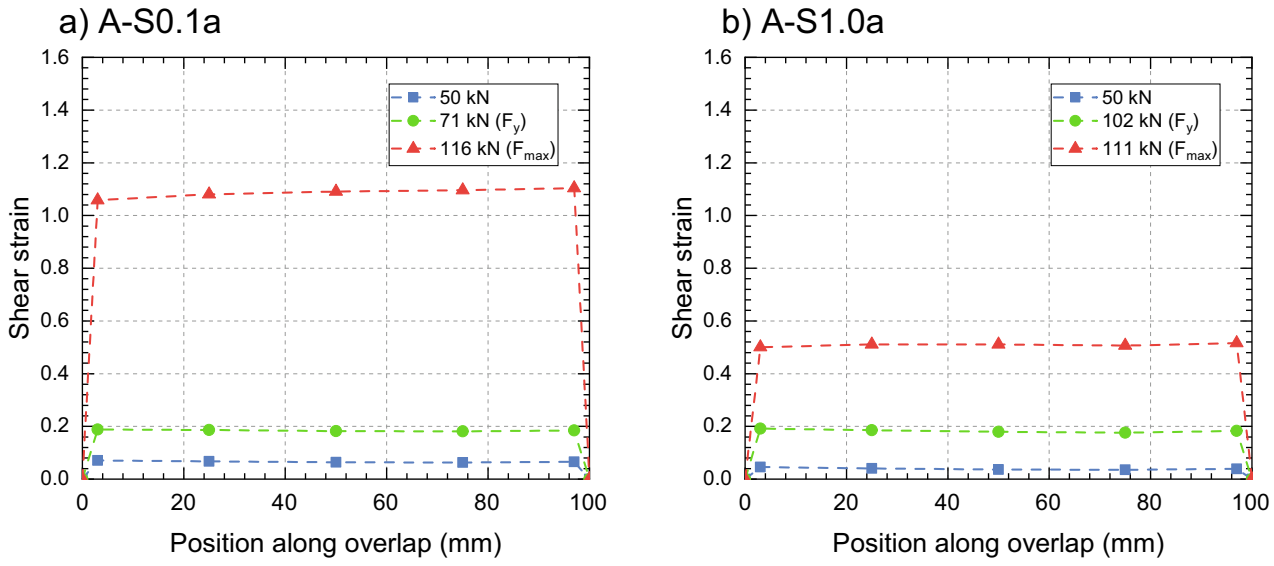

Fig. 7. Shear strain distributions along overlap of adhesive joints at different load levels, a) A-S0.1a, b) A-S1.0a.

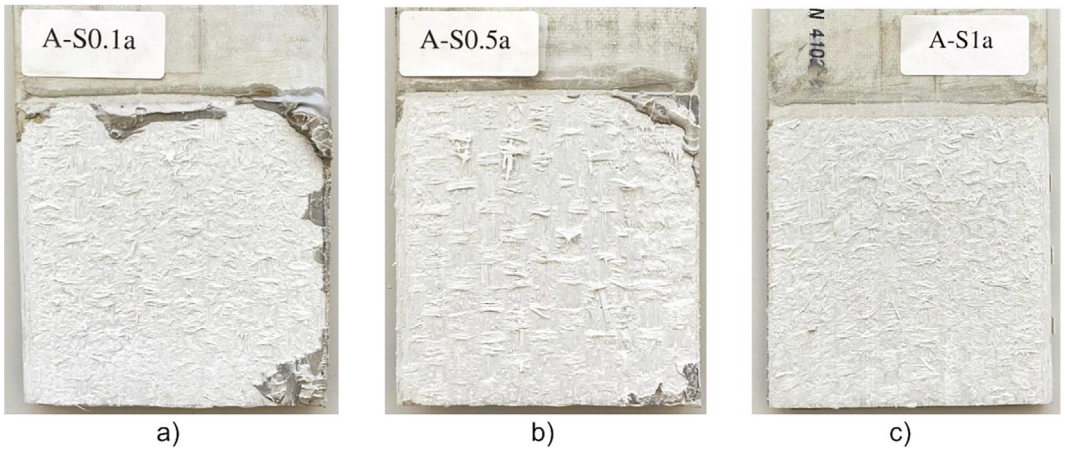

Fig. 8. Fiber-tear failure modes of adhesive joints under monotonic loading, a) A-S0.1a, b) A-S0.5a, c) A-S1.0a.

behavior); only the primary cycles are shown and their number is indicated. The trailing cycles always overlapped each other and also overlapped the subsequent primary cycle. Table 2 furthermore summarizes the maximum loads reached during each loading history, F_{max}; the joint displacements at the failure cycle, Δ_{fail}; and the cycle numbers when failure occurred, N_{fail}.

The hysteresis loops were almost tension–compression symmetric in all cases. In a first phase, the tensile and compressive reversals had a parabolic shape, i.e. the cyclic responses exhibited a softening behavior, as also occurred in the monotonic experiments. In the second phase however, the shapes changed to sigmoid, i.e. the responses showed a hardening behavior, again similar to the monotonic experi-

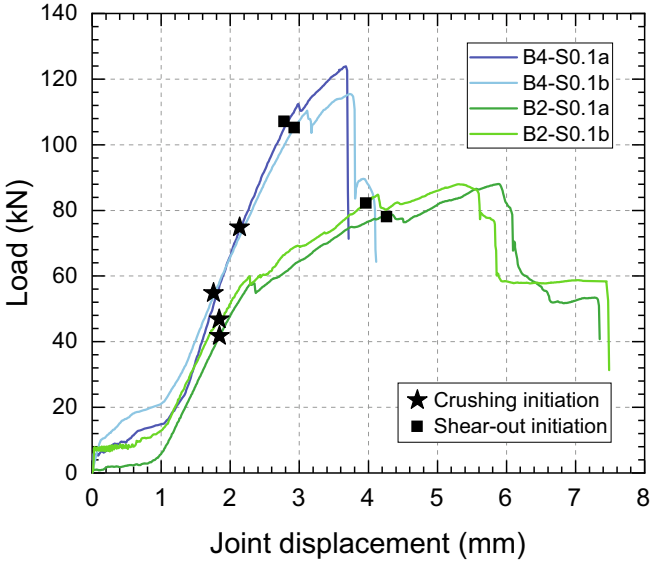

Fig. 9. Load-joint displacement responses of bolted joints.

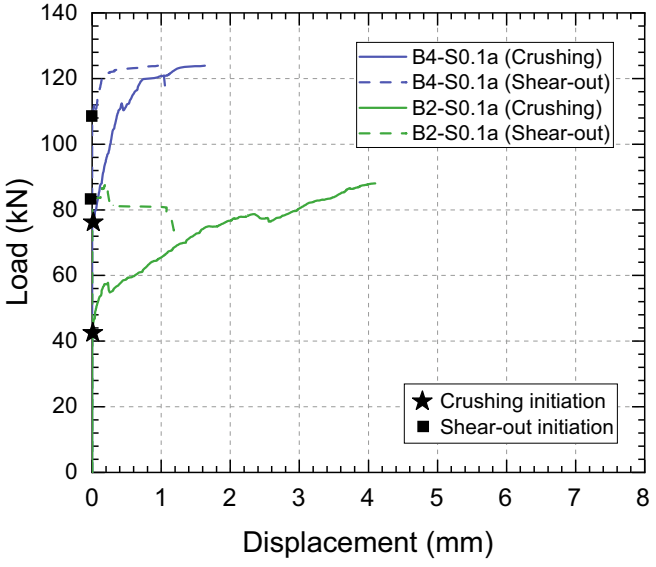

Fig. 10. Crushing and shear-out behavior of B4-S0.1a and B2-S0.1a bolted joints.

ments. The changes of these behaviors occurred in cycles no. 32 and 41 at the low and medium rates respectively, while the specimens at the high rate failed before entering the second phase. The hardening behavior was attributed to a stretching of the molecule chains and their alignment to the load direction, which was possible at the low and medium rates. In the last cycles prior to failure, subsequent to hardening and prior to the peak load, the joints again exhibited a short softening behavior.

The peak loads were similar at the low and medium rates while at the high rate they were slightly higher, see Table 2. Specimens at the medium rate exhibited the highest number of cycles up to failure, followed by those at the low and high rates. However, the displacements at failure were similar at the low and medium rates.

The envelope curves of the responses shown in Fig. 12, i.e. the curves connecting the cyclic peak loads, are presented in Fig. 13. The tension envelopes were denominated as previously explained, while the denomination of the compression envelopes was complemented by ''-c''. The envelope curves confirmed the almost symmetric behavior; they also exhibited a softening after the peak at the medium and high rates and hardening at the low rate up to the penultimate primary cycle. Two mechanisms apparently worked against each other at the low and medium rates, softening due to damage formation and hardening due to molecule chain stretching. At the low rate, hardening dominated up to the penultimate primary cycle while softening dominated at the medium rate.

Two different failure modes were observed, see Fig. 14. At the low and medium rates, cohesive failure occurred in the adhesive, while at the high rate the joints exhibited fiber-tear failure in the inner laminate, as was the case in the monotonic experiments.

3.2.2. Bolted joints

The load-joint displacement responses of the bolted joints under cyclic loading are shown in Fig. 15 (again primary cycles only) and the results are summarized in Table 2. The specimens exhibited linear behavior up to the initiation of crushing, which is indicated by star symbols in Fig. 15 and occurred on both sides of the holes, depending on tension or compression loading. The responses then became nonlinear up to the initiation of shear-out under tensile loading (indicated by square symbols). The maximum load was reached in the cycle in which shear-out initiated or in the following one. Subsequently, the load rapidly dropped in the tension cycles while under compression loading, where no shear-out was possible, the load dropped at a much lower rate. The displacements obtained from the target pairs that measured the cumulated crushing and shear-out values (see above), were almost the same as those obtained for the whole joints in Fig. 15 and are thus not shown; the only differences were the small elastic displacements of the laminates.

Prior to crushing initiation, the ''plateau'' segment without load increase, shown in each cycle, corresponded to the hole clearance. During crushing and after shear-out initiation, this plateau extended to include the cumulated crushing and shear-out deformations of the previous cycle. The small fluctuations and non-zero values of the load in the plateau region were attributed to friction between the bolts and the inside of the rugged and deformed bolt-holes.

As mentioned above, since under compression loading shear-out failure was not possible, the specimens were still able to bear load under compression, while under tension, after shear-out failure, only the plateau, caused by the bolt friction, was maintained. Failure of the specimen was thus defined at the first primary cycle where the load under tension no longer noticeably increased above the plateau value.

The envelope curves of the cyclic load-joint displacement responses are shown in Fig. 16. The denomination of the compression envelopes was again complemented by ''-c''. The envelope curves clearly showed the non-symmetric behavior, i.e. the higher peak loads in compression compared to tension, and the much faster softening in tension due to shear-out, compared to the slower softening in compression where only crushing occurred. The peak loads in the four-bolt joints were higher and the displacements at failure smaller compared to the two-bolt joints, as was also the case in the monotonic experiments for the same reasons (see above).

The failure modes of the four- and two-bolt joints are shown in Fig. 17. The crushing and shear-out patterns in the inner laminates were similar to those under monotonic loading, except that crushing occurred in both directions under cyclic loading. The crushing deformation in the two-bolt joints was much larger than in the four-bolt joints, as also shown in the much longer plateaus of the failure cycles in Fig. 15. The photos also show that the laminates were still able to bear compression loading since no shear-out could occur in that direction. Again, the outer laminates and steel bolts were not damaged.

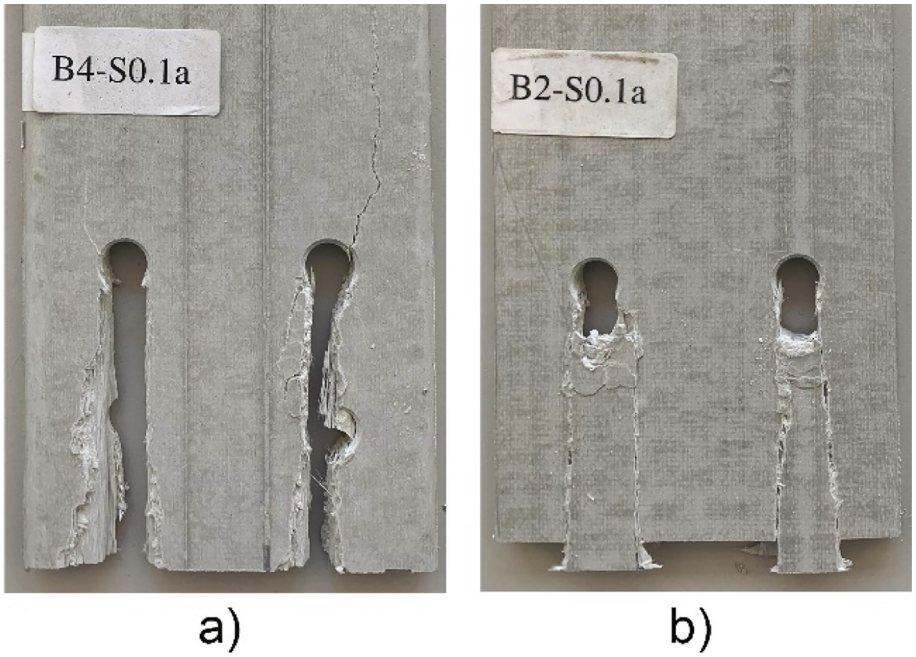

Fig. 11. Combined crushing and shear-out failure modes of bolted joints under monotonic loading, a) B4-S0.1a, b) B2-S0.1a.

Table 2
Results obtained from cyclic experiments for adhesive and bolted joints.

Specimen	Δ (mm)	F_{max} (kN)	Δ_{fail} (mm)	N_{fail}
A-C0.1a	7.15	93.7	17.5	44
A-C0.1b	7.15	90.5	17.7	44
A-C0.5a	2.90	87.8	14.3	59
A-C0.5b	2.90	94.1	14.4	59
A-C1.0a	2.30	110.1	3.2	38
A-C1.0b	2.30	109.8	3.1	38
B4-C0.1a	1.65	115.1	5.9	47
B4-C0.1b	1.65	114.7	5.8	47
B2-C0.1a	3.00	92.4	9.9	47
B2-C0.1b	3.00	91.3	8.4	44

Note: F_{max} values refer to tensile loading.

4. Discussion

4.1. Comparison of monotonic and cyclic behavior

The monotonic load–displacement responses and the tensile envelope curves of the cyclic responses of both adhesive and bolted joints are compared in Fig. 18. With regard to the adhesive joints, shown in Fig. 18(a), the monotonic and cyclic envelope curves were similar at the high rate; the peak loads and failure modes, i.e. fiber-tear, were the same, and only the displacements at the peak load and failure were smaller under cyclic loading. At the low and medium rates, however, the envelope curves were clearly below the monotonic curves because more damage was progressively accumulated during the cyclic loading compared to the monotonic loading. Since the cyclic peak loads were thus below the monotonic maximum (failure) loads, the cyclic displacements up to failure, occurring mainly in the adhesive layer, could increase compared to the monotonic displacements, particularly at the medium rate where they tripled. The failure modes thus changed from fiber-tear to cohesive failure, which occurred after damage accumulation during stretching and alignment of the adhesive's molecular chains.

In the case of bolted joints, monotonic and cyclic responses were again similar, as in the case of the high rate in the adhesive joints, see Fig. 18(b), i.e. the maximum loads were similar and only the displacements at maximum load were smaller under cyclic loading; the failure modes remained basically the same.

4.2. Stiffness degradation

The cycle-to-cycle stiffness degradation of all joints, during the tensile cycles, is shown in Fig. 19. To appropriately compare the behaviors, the cycle secant stiffnesses, K_i, were normalized by the elastic stiffnesses of the corresponding envelopes, K_e, and the cycle displacements, Δ_i, by the yield displacements, Δ_y, of the envelopes. The elastic stiffnesses and yield displacements were determined according to [22], and the results are shown in Table 3. For the bolted joints, the clearance was excluded from the displacements. The resulting rate-dependent trend of the envelope stiffnesses of the adhesive joints were similar to that of the initial stiffness, S, of the monotonic experiments, as described above, see Table 1; the latter values were however higher since the tangential stiffnesses were calculated in that case. The normalization of the stiffnesses almost led to an overlap of all degradation curves. In the adhesive joints at the low and medium rates, a rapid decrease occurred in the first damage phase at low amplitudes and high frequencies, while subsequently, during the molecular stretching, the stiffness degradation significantly slowed. The bolted joints and the adhesive joints at the high rate exhibited only one significant, almost linear, stiffness drop up to failure.

4.3. Energy dissipation capacity

4.3.1. Energy dissipation per cycle

The energy dissipation per cycle of both adhesive and bolted joints up to joint failure was determined and compared. The dissipated energy was taken equivalent to the enclosed area of the load-joint displacement hysteresis loops shown in Figs. 12 and 15. For the bolted joints, the energy dissipated by bolt friction, i.e. the areas between the two plateaus in Fig. 15, was also taken into account.

The resulting dissipated energies per cycle are shown in Fig. 20. The highest amount of energy per cycle was dissipated in the adhesive joints at the low rate, followed by the adhesive joints at the medium rate. Both curves exhibited a maximum reached before the significant

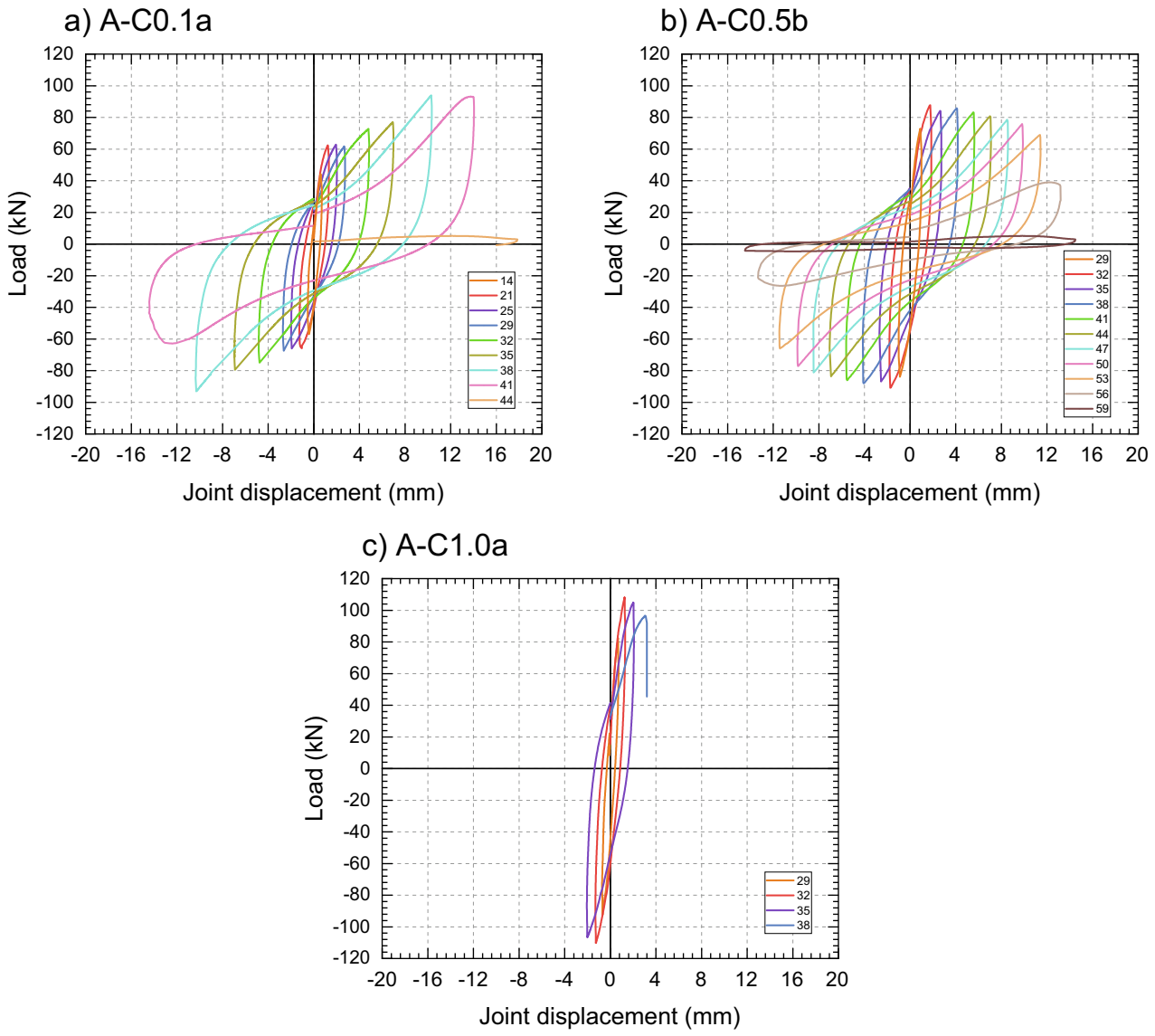

Fig. 12. Load-joint displacement responses of adhesive joints under cyclic loading, a) A-C0.1a, b) A-C0.5b, c) A-C1.0a.

drop of the load, see Fig. 12. During the last cycles preceding failure, the energy dissipated per cycle thus significantly decreased. The adhesive joints at the high rate dissipated the lowest amount of energy per cycle.

The bolted joints also exhibited a maximum energy dissipation per cycle before the values decreased. The maximum was higher for the two-bolt than for the four-bolt joints, but both were lower than the maxima of the adhesive joints at the two lower rates. The maximum energy per cycle was dissipated at the cycle after shear-out initiation.

4.3.2. Cumulative energy dissipation

The cumulative dissipated energy was obtained from the summation of the energies dissipated in all cycles, including primary and trailing cycles. For the bolted joints, the summation was stopped at the primary cycle, which no longer exhibited any noticeable load increase under tension, previously defined as joint failure. The resulting cumulative dissipated energies are shown in Fig. 21, as a function of the number of cycles (a), and joint displacements (b).

The largest amounts of cumulative energy were dissipated by the adhesive joints at the low and medium rates, while the joints at the medium rate dissipated more energy than those at the low rate, see Fig. 21. At a certain cycle, however, the joints at the low rate dissipated more energy than those at the medium rate, as shown in Fig. 21(a), since the imposed displacements were higher (see reference displacements in Table 1). At the same imposed displacement however, the joints at the low rate dissipated less energy, as shown in Fig. 21(b), since fewer cycles were completed than in the joints at the medium rate. Finally, since, independent of the rate, both joints failed at almost the same displacement – achieved mainly in the adhesive layer – the joints at the medium rate and fewer imposed displacements per cycle were able to sustain more cycles and thus dissipated more energy. The lowest amount of energy was dissipated in the adhesive joints subjected to the high displacement rate, since the adhesive was not able to enter the second branch of its bilinear behavior and thus to dissipate a significant amount of energy.

The bolted joints dissipated much less energy than the adhesive joints subjected to the low and medium rates. The two-bolt joints dissipated more energy per cycle than the four-bolt joints, see Fig. 21(a), since the imposed joint displacements per cycle were larger (see Table 1). These displacements were directly transformed into crushing and shear-out deformations. On the other hand, for the same imposed joint displacement, the two-bolt joints dissipated less energy than the

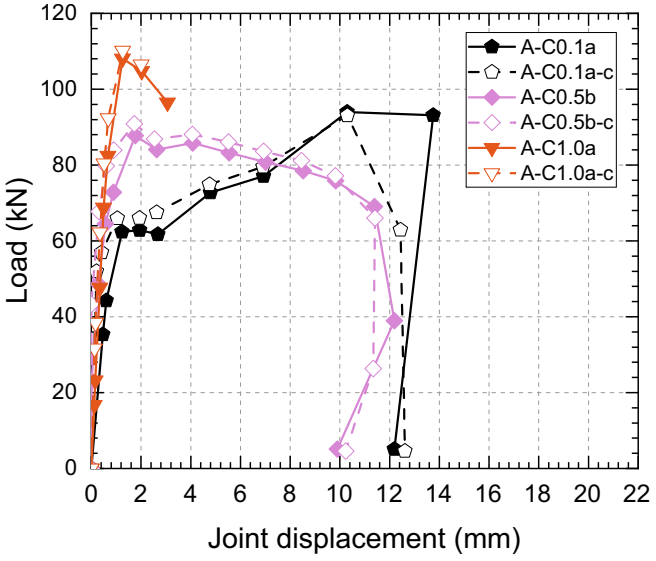

Fig. 13. Envelope curves of load-joint displacement responses of adhesive joints.

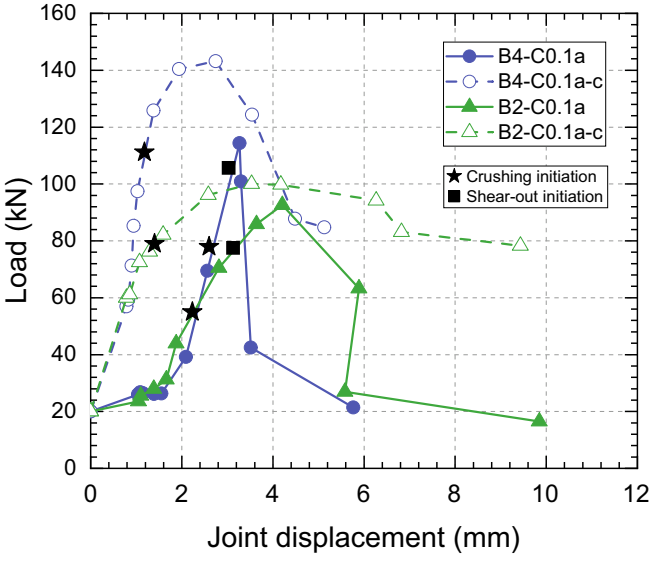

Fig. 16. Envelope curves of load-joint displacement responses of bolted joints.

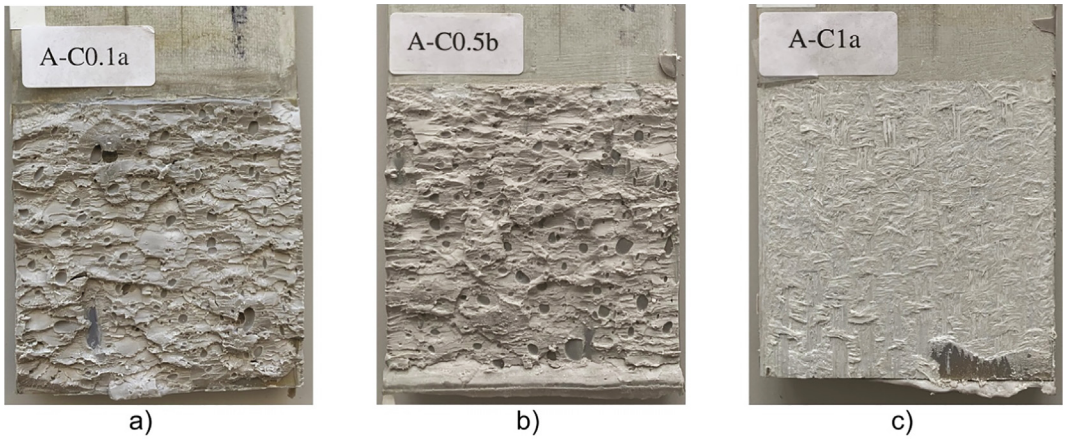

Fig. 14. Failure modes of adhesive joints under cyclic loading, cohesive failure in a) A-C0.1a and b) A-C0.5b, fiber-tear failure in c) A-C1.0a.

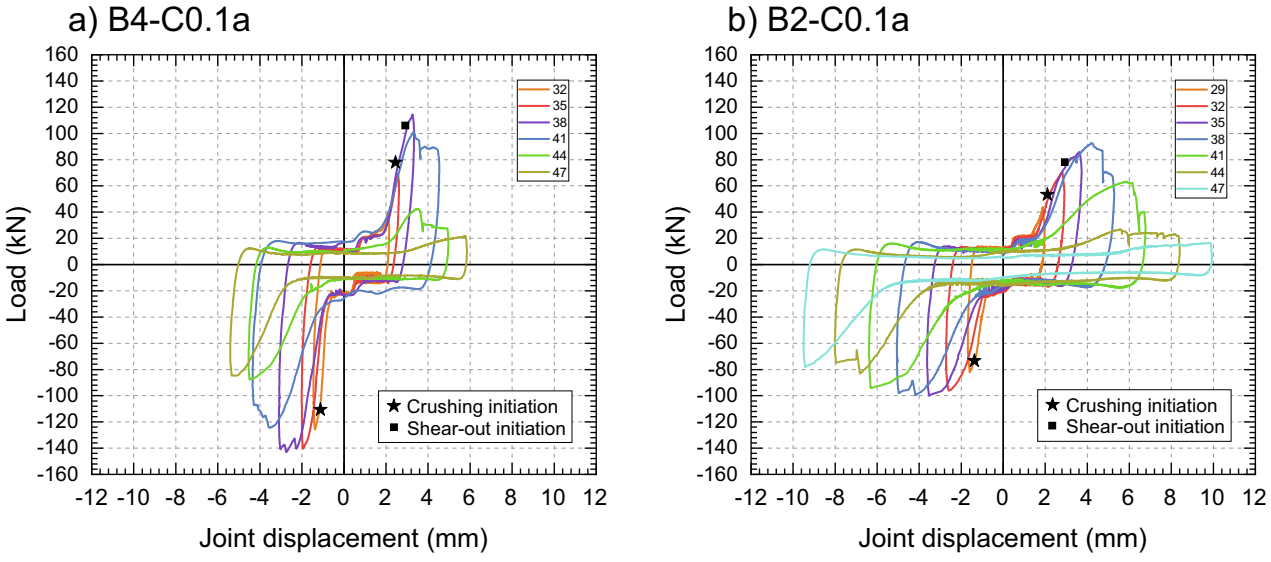

Fig. 15. Load-joint displacement responses of bolted joints under cyclic loading, a) B4-C0.1a, b) B2-C0.1a.

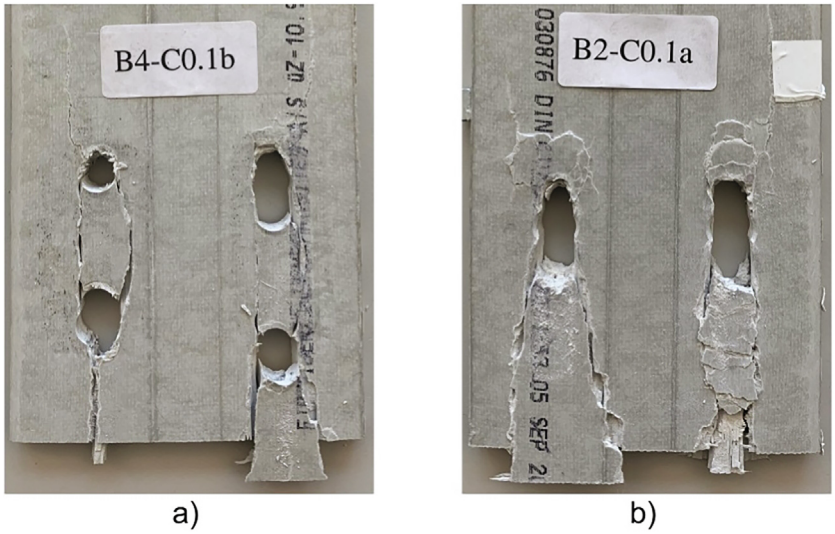

Fig. 17. Combined crushing and shear-out failure modes of bolted joints under cyclic loading, a) B4-C0.1b b) B2-C0.1a.

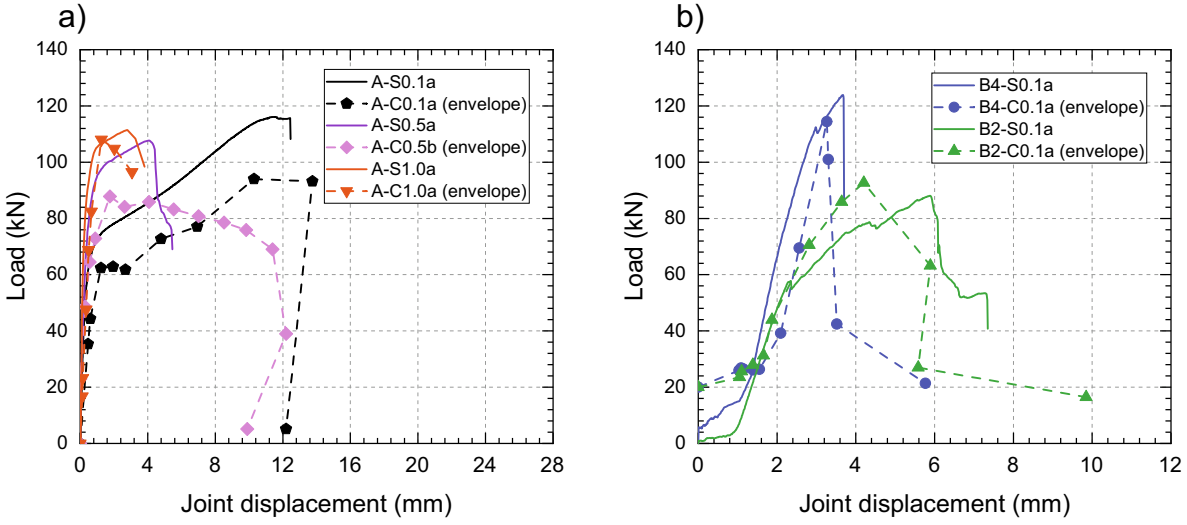

Fig. 18. Comparison of monotonic load-joint displacement curves and tensile cyclic loading envelope for a) adhesive and b) bolted joints.

four bolt joints, as shown in Fig. 21(b), since the same crushing and shear-out deformation was produced only twice (by two bolts) and not four times (by four bolts). Due to the longer laminate length between bolts and laminate ends, the two-bolt joints were able to sustain much larger displacements up to failure and thus finally dissipated more energy than the four-bolt joints, although they exhibited a significantly lower monotonic strength (under tension).

In adhesive joints, an optimum displacement rate seems to exist, at which a maximum number of cycles can be sustained by the joint while the adhesive still maintains a high deformation capacity, see Fig. 22. On the other hand, an adhesive can also be designed or selected accordingly, adapted to the design displacement rate, in order to dissipate a maximum amount of energy.

4.3.3. Normalized energy dissipation

The energy dissipated per cycle was normalized by the input energy, i.e. the sum of the elastic and dissipated energy, in order to further compare the different joints, as shown in Fig. 23. In all the joints, at least approximately 90% of the input energy was dissipated, reaching almost 100% towards failure. Closer investigation, however, permitted further differentiation of the energy share of the different

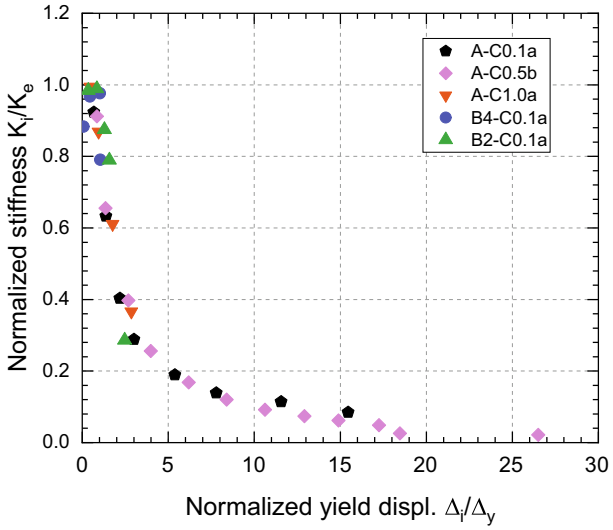

Fig. 19. Normalized cycle-to-cycle stiffness degradation as a function of normalized displacement.

damage mechanisms. The adhesive joints exhibited two maxima and a minimum of normalized energy dissipation in between, as shown in Fig. 23(a). The first maximum was obtained during damage formation at small amplitudes and high frequencies where the elastic energy portion was small. With increasing deformation at lower frequencies, stretching of the molecule chains became dominant and the elastic energy portion increased, i.e. the dissipated/input energy ratio decreased and reached a minimum. In the last cycles before failure, damage again became dominant and the dissipated energy portion increased and the ratio exhibited the second maximum. The three stages coincided well with the consecutive softening-hardening–softening behavior discussed in Section 3.2.1 based on Fig. 12. The first two stages also agreed well with the trend of stiffness degradation shown in Fig. 19, i.e. significant stiffness drop during the first damage phase and leveling-off of stiffness degradation during molecular stretching.

In the bolted joints, the first cycles were dominated by friction of the bolt in the hole, i.e. the whole input energy was dissipated (ratio of 1.0). Subsequently elastic deformation became significant and the ratio decreased. With the initiation of crushing, the decreasing trend was halted, and the dissipated energy became dominant and the ratio increased during crushing and shear-out up to failure.

Table 3
Elastic stiffness and yield displacement of envelopes determined according to [19].

Specimen	K_e (kN/mm)	Δ_y (mm)
A-C0.1a	80	0.89
A-C0.1b	94	0.79
A-C0.5a	124	0.76
A-C0.5b	125	0.66
A-C1.0a	141	0.71
A-C1.0b	154	0.66
B4-C0.1a	65	1.24
B4-C0.1b	64	1.42
B2-C0.1a	29	1.90
B2-C0.1b	33	0.90

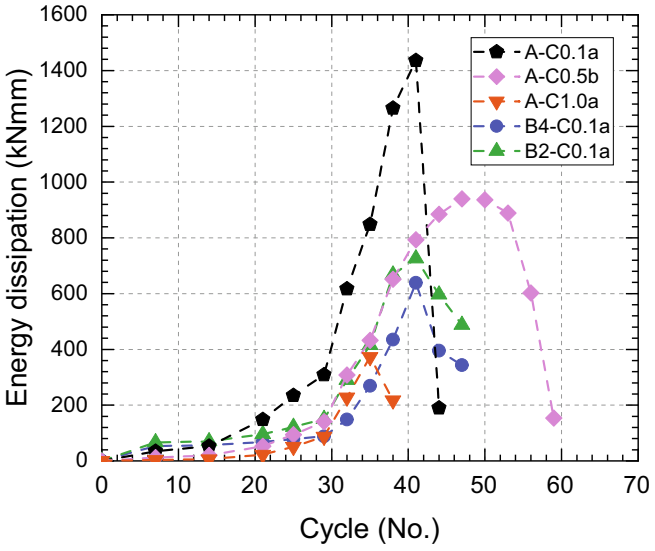

Fig. 20. Energy dissipation per cycle of adhesive and bolted joints up to failure.

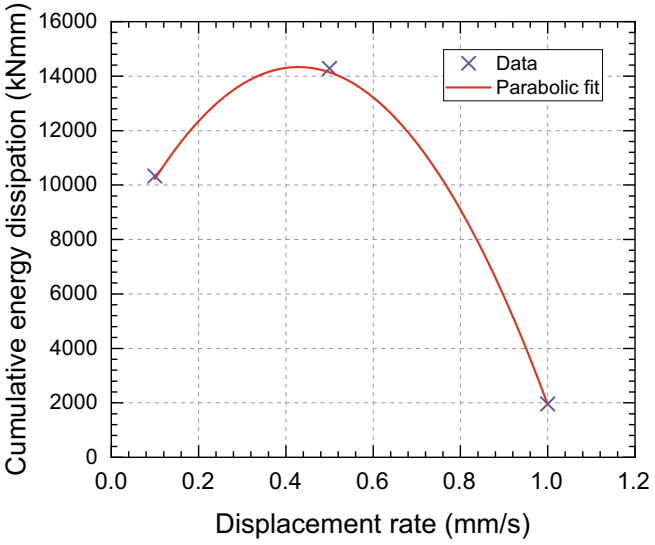

Fig. 22. Dissipated cumulative energy as a function of displacement rate for adhesive joints.

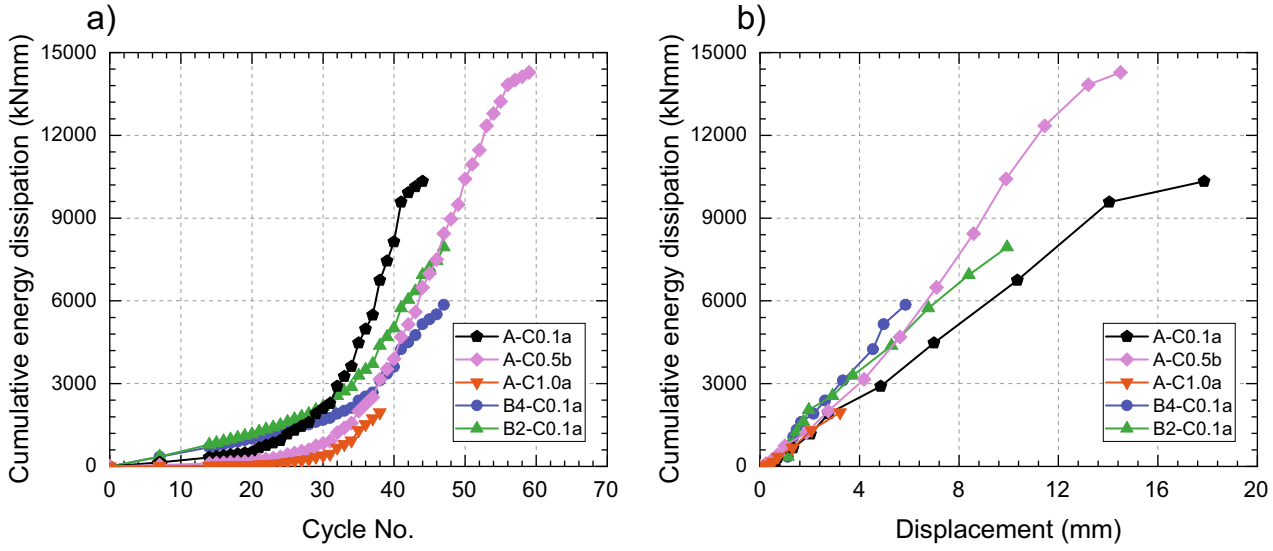

Fig. 21. Cumulative energy dissipation of adhesive and bolted joints up to failure, as a function of a) cycle number, b) joint displacement.

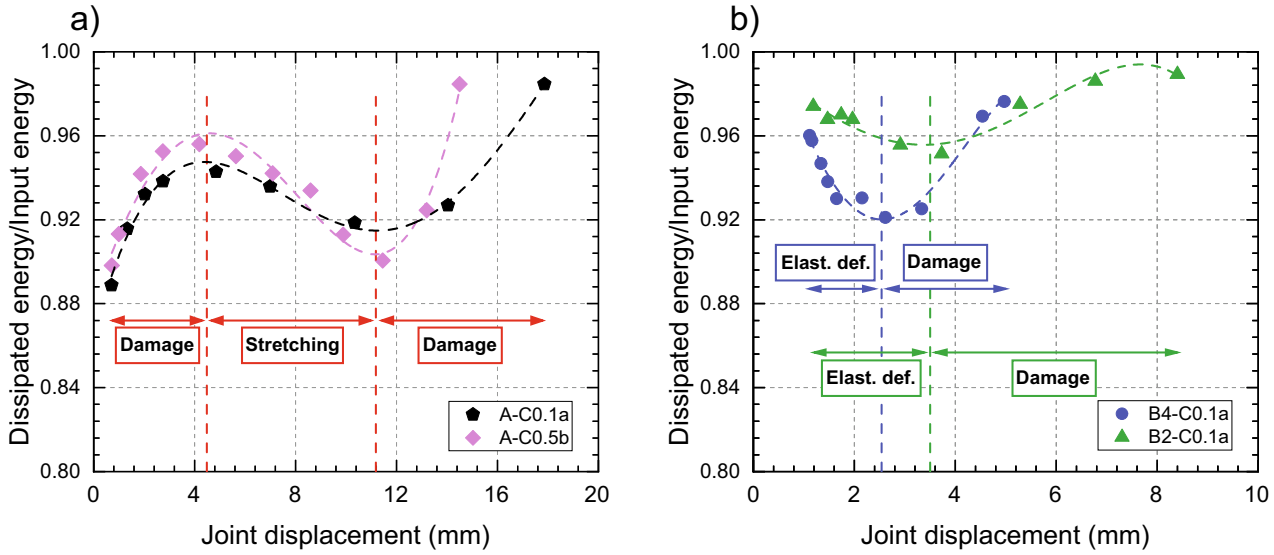

Fig. 23. Energy dissipation per cycle normalized by input energy as a function of joint displacement for a) adhesive and b) bolted joint, dominant mechanisms are indicated.

5. Conclusions

Monotonic tension and reversed cyclic loading experiments were performed on adhesive and bolted double-lap joints composed of pultruded GFRP profiles. A flexible adhesive and two or four steel bolts were used in the adhesive and bolted joints, respectively. The joint dimensions in all configurations were similar and the monotonic strengths of the adhesive and four-bolt joints were also similar, only those of the two-bolt joints were slightly lower. The effects of the displacement rate in the adhesive joints and the bolt configuration in the bolted joints on the energy dissipation capacity were investigated and adhesive and bolted joints were compared in this respect. The conclusions from this experimental investigation are as follows:

1- A significant amount of energy was dissipated in the adhesive joints by viscoelastic friction, including molecular chain stretching and damage in the adhesive layer at lower and medium joint displacement rates, while almost no energy dissipation occurred at the highest rate.
2- Energy in the bolted joints was dissipated by progressive crushing and shear-out failures in the inner laminates. Two-bolt joints dissipated significantly more energy than four-bolt joints, although their monotonic strength was lower, mainly due to the longer edge distances in the two-bolt joints.
3- The adhesive joints subjected to the two lower displacement rates dissipated significantly more energy than the bolted joints although the joint dimensions were similar and their monotonic strength was similar or only slightly higher than that of the four- or two-bolt joints, respectively.
4- In adhesive joints an optimum displacement rate was observed, at which a maximum amount of energy was dissipated. Furthermore, a higher portion of the input energy was dissipated and stiffness degradation was more pronounced during predominant damage formation than during predominant molecular stretching.

6. Data availability statement

The raw/processed data required to reproduce these findings cannot be shared at this time as the data also forms part of an ongoing study.

CRediT authorship contribution statement

Ghazaleh Eslami: Conceptualization, Investigation, Formal analysis, Writing - original draft. **Sonia Yanes-Armas:** Conceptualization, Validation, Writing - review & editing. **Thomas Keller:** Conceptualization, Validation, Writing - review & editing, Supervision.

Declaration of Competing Interest

The authors declare that they have no known competing financial interests or personal relationships that could have appeared to influence the work reported in this paper.

Acknowledgements

The authors would like to thank SIKA AG, Switzerland (adhesive supplier) and Fiberline Composites A/S, Denmark (pultruded laminate supplier) for their support of this research.

References

[1] Keller T, De Castro J. System ductility and redundancy of FRP beam structures with ductile adhesive joints. Compos Part B Eng 2005;36:586–96. https://doi.org/10.1016/j.compositesb.2005.05.001.
[2] Keller T, Gürtler H. Composite Action and Adhesive Bond between Fiber-Reinforced Polymer Bridge Decks and Main Girders. J Compos Constr 2005;9:360–8. https://doi.org/10.1061/(ASCE)1090-0268(2005)9:4(360).
[3] Yanes-Armas S, de Castro J, Keller T. Energy dissipation and recovery in web–flange junctions of pultruded GFRP decks. Compos Struct 2016;148:168–80. https://doi.org/10.1016/j.engstruct.2017.03.003.
[4] Angelidi M, Vassilopoulos AP, Keller T. Ductile adhesively-bonded timber joints – Part 1: Experimental investigation. Constr Build Mater 2018;179:692–703. https://doi.org/10.1016/j.conbuildmat.2018.05.214.
[5] Avendaño R, Carbas RJC, Marques EAS, da Silva LFM, Fernandes AA. Effect of temperature and strain rate on single lap joints with dissimilar lightweight adherends bonded with an acrylic adhesive. Compos Struct 2016;152:34–44. https://doi.org/10.1016/j.compstruct.2016.05.034.
[6] Fiberline Composites, Fiberline Design Manual, (2003).
[7] Othman AR, Jadee KJ. Specific bearing strength of bolted composite joint with different glass fiber reinforcement. ARPN J Eng Appl Sci 2016;11:12039–44.
[8] Gattesco N, Gubana A, Buttazzi M, Melotto M. Experimental investigation on the behavior of glued-in rod joints in timber beams subjected to monotonic and cyclic loading. Eng Struct 2017;147:372–84. https://doi.org/10.1016/j.engstruct.2017.03.078.
[9] Žarnić R, Rajčić V, Kržan M. Response of laminated glass-CLT structural components to reverse-cyclic lateral loading. Constr Build Mater 2020;235. https://doi.org/10.1016/j.conbuildmat.2019.117509.

[10] Ye J, Mojtabaei SM, Hajirasouliha I. Seismic performance of cold-formed steel bolted moment connections with bolting friction-slip mechanism. J Constr Steel Res 2019;156:122–36. https://doi.org/10.1016/j.jcsr.2019.01.013.
[11] Dai L, Zhao X, Rasmussen KJR. Cyclic performance of steel storage rack beam-to-upright bolted connections. J Constr Steel Res 2018;148:28–48. https://doi.org/10.1016/j.jcsr.2018.04.012.
[12] Xiao X, Zhang Z, Bai Y. Comparative study of energy dissipation capacity of steel and glass fibre-reinforced polymer frames with bonded sleeve connections. J Reinf Plast Compos 2017;36:1665–79. https://doi.org/10.1177/0731684417723714.
[13] Zhang Z, Bai Y, He X, Jin L, Zhu L. Cyclic performance of bonded sleeve beam-column connections for FRP tubular sections. Compos Part B Eng 2018;142:171–82. https://doi.org/10.1016/j.compositesb.2018.01.024.
[14] Qiu C, Bai Y, Cai Z, Zhang Z. Cyclic performance of splice connections for hollow section fibre reinforced polymer members. Compos Struct 2020;243:. https://doi.org/10.1016/j.compstruct.2020.112222112222.
[15] Martins D, Proença M, Almeida Gonilha J, Figueiredo Sá M, Ramôa Correia J, Silvestre N. Experimental and numerical analysis of GFRP frame structures. Part 1: Cyclic behaviour at the connection level. Compos Struct 2019;220:304–17. https://doi.org/10.1016/j.compstruct.2019.03.097.
[16] Keller T, Rothe J, de Castro J, Osei-Antwi M. GFRP-Balsa Sandwich Bridge Deck: Concept, Design, and Experimental Validation. Compos Constr 2014;18:10–20. https://doi.org/10.1061/(ASCE)CC.1943-5614.
[17] Angelidi M, Vassilopoulos AP, Keller T. Ductility, recovery and strain rate dependency of an acrylic structural adhesive. Constr Build Mater 2017;140:184–93. https://doi.org/10.1016/j.conbuildmat.2017.02.101.
[18] H. Krawinkler, F. Parisi, L. Ibarra, A. Ayoub, R. Medina, Development of a Testing Protocol for Woodframe Structures, CUREE Publ. No. W-02. (2001) 1–76. https://www.curee.org/publications/woodframe/downloads/CUREEpub_W-02.pdf%0Awww.curee.org.
[19] ASTM Standard E2126, 2019, Standard Test Methods for Cyclic (Reversed) Load Test for Shear Resistance of Vertical Elements of the Lateral Force Resisting Systems for Buildings, ASTM Int. West Conshohocken, PA,. (2019) 1–15. Doi: 10.1520/E2126—19.
[20] Iso 1667:2003, Timber structures — Joints made with mechanical fasteners — Quasi-static reversed-cyclic test method, (2003). https://www.iso.org/standard/31041.html.
[21] ASTM D5573, Standard Practice for Classifying Failure Modes in Fiber-Reinforced-Plastic (FRP), (2012). Doi: 10.1520/D5573-99R12.2.
[22] CEN12512, Timber structures – test methods – cyclic testing of joints made with mechanical fasteners [including amendment A1:2005], BS EN 1251 (2005). http://canterbury.summon.serialssolutions.com.